K.-D. Gottschaldt, U. Walzer, D. R. Stegman, J. R. Baumgardner, and H.-B. Mühlhaus. Mantle Dynamics - A Case Study. In Huilin Xing, ed. Advances in Geocomputing, Lecture Notes in Earth Sciences, Vol. 119, pp. 139-181, Springer, 2009.

V. Mantle Dynamics – A Case Study

Klaus-D. Gottschaldt,[1] Uwe Walzer,[2] Dave R. Stegman,[3]
John R. Baumgardner[4] and Hans B. Mühlhaus[5]

[1]University of Queensland, ESSCC, PO Box 6067, St Lucia, QLD 4067, Australia; now at: Deutsches Zentrum Für Luft- und Raumfahrt, Institut Für Physik der Atmosphäre, 82234 Oberpfaffenhofen, Germany
[2]Friedrich-Schiller-Universität Jena, Institut für Geowissenschaften, Burgweg 11 07749 Jena, Germany
[3]Earth Sciences, The University of Melbourne, Victoria 3010, Australia
[4]University of California, Department of Earth & Planetary Science, 307 McCone Hall, Berkeley, CA 94720-4767, USA
[5]University of Queensland, ESSCC, PO Box 6067, St Lucia QLD 4067, Australia

E-mail: klausgottschaldt@web.de

Abstract Solid state convection in the rocky mantles is a key to understanding the thermochemical evolution and tectonics of terrestrial planets and moons. It is driven by internal heat and can be described by a system of coupled partial differential equations. There are no analytic solutions for realistic configurations and numerical models are an indispensable tool for researching mantle convection. After a brief general introduction, we introduce the basic equations that govern mantle convection and discuss some common approximations. The following case study is a contribution towards a self-consistent thermochemical evolution model of the Earth. A crude approximation for crustal differentiation is coupled to numerical models of global mantle convection, focussing on geometrical effects and the influence of rheology on stirring. We review Earth-specific geochemical and geophysical constraints, proposals for their reconciliation, and discuss the implications of our models for scenarios of the Earth's evolution. Specific aspects of this study include the use of passive Lagrangian tracers, highly variable viscosity in 3-d spherical geometry, phase boundaries in the mantle and a parameterised model of the core as boundary condition at the bottom of the mantle.

H. Xing, *Advances in Geocomputing*, Lecture Notes in Earth Sciences 119,
DOI 10.1007/978-3-540-85879-9_5

1 Introduction

Terrestrial planets like the Earth, Mars and Venus consist of a metallic core and a silicic mantle. The rocky mantles can be partially molten in small regions, but the vast majority of the mantle material is solid. In response to short-term force (e.g. seismic waves) the mantle behaves like an elastic solid body. However, in geological time scales the rock behaves like a viscous fluid. Thermal and thermo-chemical convection is possible on a range of scales. Mantle convection provides a framework to reconcile observations of planetary magnetic and gravity fields, heat flux, distribution of volcanoes and tectonic structures, geo- & cosmochemistry and mineral physics. Numerical models are an indispensable tool for researching mantle convection.

1.1 Energy Budget of the Mantle

Thermal convection in terrestrial bodies is driven by internal heat sources. This heat stems from accretion, the decay of radioactive elements, tidal dissipation, and the gravitational energy which is released during the differentiation into core, mantle and crust. The relative importance of each of these heat sources is a function of time and can vary from one terrestrial body to another. Please note: although solar irradiation can be orders of magnitude bigger than internal heat, it has no effects on internal dynamics. Solar irradiation penetrates less than a few 100 m, driving only processes close to the surface. In contrast, phenomena like volcanism, planetary magnetism, tectonics and seismicity are controlled by internal heat.

1.2 Physics of Mantle Convection in a Nutshell

Mantle dynamics can be described by the equations for the conservation of energy, momentum and mass, equation(s) of state, initial and boundary conditions. Solid state creep in the mantle is very slow, in the order of centimetres per year. Therefore inertia is negligible, but frictional terms and constitutive relations are crucial for the fluid dynamics of the mantle. Mantle rheology strongly depends on temperature and pressure and is not very well constrained.

1.3 Surface Tectonics

Tectonics is the manifestation of internal dynamics at the outer boundary layer of the mantle. The simplest tectonic regime is a freely deformable surface, a so-called mobile lid. Fluids with low viscosity contrasts – like oceans – display this behaviour, but it is not known from any solid mantle. In contrast, a steep viscosity increase towards the surface produces a stagnant lid. Convection just takes place in the mantle below the lid. Mars and the Moon are examples for this tectonic style. The Earth is the only known planet currently operating plate tectonics. Here the outer lid is broken into several plates that show little internal deformation, but change their shapes and relative positions. Plate material is generated at divergent margins and recycled into the mantle at convergent zones. The tectonic style of a planet may change and the controlling parameters are a current research topic.

1.4 Volcanism

Apart from the tectonic style, the distribution of volcanoes is another characteristic feature of each planet. On Earth, most volcanic activity occurs along the rims of tectonic plates, sampling the shallow mantle. Additionally there are at least 32 rising plumes that sample the deep mantle (Montelli et al. 2004; Davies 2005). Plumes move much slower laterally than tectonic plates and therefore appear to be stationary relative to each other. Strongly reduced viscosity in those 'hot spots' permits rising velocities in the order of 10 cm/yr, in narrow conduits of a few 100 km in diameter. On Earth, plume locations seem to be related to large upwellings in the lower mantle, under Africa and the Pacific (McNamara and Zhong 2004). Plumes and plate tectonics are modes of heat transport within and out of the mantle, but their relative importance is not entirely clear (Nolet et al. 2006).

There are only two narrow volcanic centres on Mars and the distribution of volcanoes on Venus seems to be random. The differences are hard to explain, particularly since narrow, hot plumes cannot be resolved satisfactorily in global mantle convection models yet.

1.5 Core and Magnetism

The evolution of the metallic core is an important boundary condition and constraint for mantle models. If the heat flux across the core mantle boundary is high enough, convection in a molten core can generate a magnetic field. This field may be preserved in rock just cooling below the

Curie point, thus providing an observational record of the magnetic field history. Core convection acts on much smaller time- and length-scales, but parameterised core models can be coupled to mantle evolution models.

1.6 Composition

Planetary mantles are a mixture of minerals and the main chemical components may be inhomogeneous on different scales. However, the resulting variation of parameters relevant to mantle convection (e.g. density, thermal conductivity) is small. Here we consider only one major component: the bulk composition of the mantle.

A more comprehensive presentation of the various aspects of mantle convection can be found in text books like Schubert et al. (2001).

2 Physics of Mantle Convection: Basic Equations

We distinguish among several types of computational models. A scaling law describes the efficiency of heat transport in parameterised models. Only a global energy budget is considered in this case, which is computationally inexpensive. These models are useful for investigating a wide parameter space. If one is interested in further details, e.g. convection structure and temperature fields, the full system of equations must be solved. Usually this is done in 2-d or 3-d, Cartesian or spherical geometry. Of those, 2-d Cartesian models generally consume the least computational resources, but 3-d spherical models are most realistic. The choice depends on the specific problem. In the following we start from general formulations of the equations to show the approximations used for mantle dynamics.

2.1 Conservation of Mass

Mass conservation is given by

$$\frac{\partial \rho}{\partial t} + \nabla \left(\rho \vec{v} \right) = 0 \tag{1}$$

with density ρ, time t, velocity $\vec{v}$ and the operator $\nabla = \frac{\partial}{\partial x_i} \vec{e}_i$.

Mantle convection is slow and density does not change rapidly. Therefore the first term can be neglected, giving the so-called anelastic liquid approximation,

$$\nabla(\rho\vec{v}) = 0 \tag{2}$$

Mantle rock is compressible. This is relevant for big terrestrial planets like the Earth, but not for the limited pressure range in smaller bodies (e.g. Moon). Equation (2) simplifies to

$$\nabla\vec{v} = 0 \tag{3}$$

for incompressible calculations.

2.2 Conservation of Momentum

The change of momentum of a small mantle element is balanced by forces acting on the element surface (pressure gradients, viscous forces) and body forces (e.g. gravity – incl. centrifugal force, Coriolis force)

$$\rho\frac{D\vec{v}}{Dt} = -\nabla p + \nabla\tau + \rho\vec{g} - 2\rho\vec{\omega}\times\vec{v} \tag{4}$$

where p is pressure, τ is the deviatoric stress tensor, $\vec{g}$ is gravity, $\vec{\omega}$ angular velocity and the material derivative $\frac{D}{Dt} = \frac{\partial}{\partial t} + \vec{v}\cdot\nabla$ (Euler system). Small mantle creep velocities allow the neglection of inertia, leading to

$$0 = -\nabla p + \nabla\tau + \rho\vec{g} \tag{5}$$

2.3 Conservation of Energy

Introducing specific heat at constant volume c_V, thermal expansivity $\alpha = -\frac{1}{\rho}\left(\frac{\partial\rho}{\partial T}\right)_p$, bulk modulus K_T, thermal conductivity k and heat generation rate per unit volume H, the energy equation is

$$\rho c_V\frac{DT}{Dt} - \frac{\alpha K_T}{\rho}T\frac{D\rho}{Dt} = \nabla(k\nabla T) + \tau\nabla\vec{v} + \rho H \tag{6}$$

The source terms on the right hand side are thermal conduction, frictional heating and volumetric heating, respectively. The second term on the left hand side vanishes for incompressible calculations.

2.4 Equation of State

Furthermore we need an equation of state to reduce the number of independent thermodynamic variables (here: p, ρ, T). Those variables vary much more radially than laterally in planetary mantles. Therefore it is convenient to consider lateral variations as a perturbation to radial reference profiles (p_r, ρ_r, T_r). The basic – but widely used – equation of state for this approach is

$$\rho = \rho_r \cdot \left[1 - \alpha(T - T_r) + \frac{p - p_r}{K_T} \right] \tag{7}$$

Only a reference point (ρ_0, T_0) is needed for the incompressible case and Eq. (7) simplifies to

$$\rho = \rho_0 \cdot \left[1 - \alpha(T - T_0) \right] \tag{8}$$

2.5 Constitutive Relations

Constitutive equations relate stress τ and deformation ε or deformation rate $\dot{\varepsilon}$. This so-called rheology strongly depends on the actual mantle conditions, may be complicated and uncertain. We show just some simple or often used examples.

Elastic behaviour

$$\tau_{ij} = E \cdot \varepsilon_{ij} \tag{9}$$

may be important for short and medium term processes near the surface, but is secondary for long term processes in the deep mantle.

Models of mantle convection often use linear viscous rheology

$$\rho \cdot H_{cool} = \rho \cdot c_v \cdot \frac{d(T - T_m)}{dt} \tag{10}$$

Here $\dot{\varepsilon}_{ij} = \frac{1}{2}\left(\frac{\partial v_i}{\partial x_j} + \frac{\partial v_j}{\partial x_i} \right)$ is the strain rate tensor and η is the shear viscosity. We have neglected volume viscosity, but η may vary, e.g. according to an Arrhenius-type equation,

$$\eta = \eta_0 \exp\left[\xi \frac{T_m}{T}\right] \tag{11}$$

Based on high-pressure experiments it has been suggested (Boehler 2000) that this viscous rheology (with mantle specific constitutive parameters combined to $\xi \approx 17$, melting temperature T_m and a reference viscosity η_0) is a good approximation for diffusion creep, the most important deformation mechanism in the Earth's lower mantle. Dislocation climb dominates in the Earth's upper mantle, resulting in a power law rheology of the form

$$\tau \sim \dot{\varepsilon}^n \tag{12}$$

According to Eq. (11), the low temperatures near planetary surfaces would result in an unrealistically rock strength. In reality rock yields above a certain threshold stress τ_y. Combining this plastic stress limiter with the viscous rheology (10) gives the effective visco-plastic viscosity

$$\eta_{eff} = \min\left[\eta(p,T), \frac{\tau_y}{2\sqrt{\dot{\varepsilon}_{II}}}\right] \tag{13}$$

Such a rheology allows strain localisation, which is a prerequisite for plate tectonics.

The six scalar Eqs. (2) or (3), (5), (6) and (7) or (8) are used to determine *T, p,* ρ and the three components of $\vec{v}$ for mantle parameters. Heating mode, boundary conditions, initial conditions, rheology, radial reference profiles and other specific parameters are discussed with the case study in the following section.

3 Case Study: Stirring in Global Models of the Earth's Mantle

This case study is a contribution towards a self-consistent thermochemical evolution model of the Earth. An approximation for crustal differentiation is coupled to numerical models of global mantle convection, focussing on geometrical effects and the influence of rheology on stirring. This section is based on Gottschaldt et al. (2006).

First we review some Earth-specific geochemical and geophysical constraints, as well as proposals for their reconciliation. Thereafter we describe

extensions to the base methodology of the previous section and the numerical approach. The results of selected models will be discussed. We highlight results that could be relevant for the Earth in the final section.

3.1 Background

3.1.1 Mantle Composition and Crustal Segregation

The following five Oxides make up 98.5% of the *bulk composition* of the Earth's mantle and crust (O'Neill et al. 1998): MgO (36.3%), Al_2O_3 (4.7%), Si_2O_3 (45.6%), CaO (3.7%), FeO (8.2%). Depending on pressure, temperature and differentiation history, these oxides form mixtures of different minerals.

Partial melt is extracted from the mantle and upon solidification forms the crust. Hence the crust is an end product of mantle differentiation. On Earth there are two chemically distinct sorts of crust. Thin (0–7 km), dense and mafic oceanic crust (OC) is continuously generated at mid-ocean ridges and recycled almost entirely back into the mantle at subduction zones. By contrast, andesitic continental crust (CC) is less dense and thicker (~40 km). It is buoyant and recycled into the mantle only to a small degree, as sediments or by delamination. While the lifetime of OC is about 100 Ma, that of CC is at least 2 Ga (Hofmann 1997). Suggestions for the segregation history of CC range from rapid early net growth to episodic growth of juvenile CC to continuous net growth (Arndt 2004). Today CC is produced mainly by andesitic volcanism related to subduction and the release of water from the slab. Continents themselves also grow through intraplate volcanism and the accretion of sediments and basaltic terranes. Such terranes could be the product of extensive melting caused by plume heads reaching the surface (Hofmann 1997). Tectonic settings for the formation of Archean cratons may have been different and include rifts (Trendall 2002), (van Thienen 2003), but are still represent on the extraction of partial melt from the shallow (<200 km: (Presnall et al. 2002)) mantle.

3.1.2 Phase Transitions in the Mantle

Olivine transforms into β-spinel at a mean depth of 410 km, γ-spinel to perovskite plus magnesiowüstite at 660 km depth. Olivine and spinel make up 58% of the upper mantle in the respective depth ranges. The other two major phases in the upper mantle undergo phase changes in the same depth range: pyroxenes and garnet change relative proportions throughout the upper mantle and gradually transform into perovskites between 600 and

700 km depth. The mantle below 700 km consists of 80% perovskite and 20% magnesiowüstite, with chemical heterogeneities of a few percent (Trampert et al. 2004). There is only one major phase transition in the lower mantle: perovskite transforms into postperovskite (ppv) near the core-mantle boundary (CMB).

Of all phase changes in the mantle (Table 1), the γ-spinel transition at 660 km depth has the biggest impact on the physical properties and dynamics of the mantle. It defines the boundary between upper (UM) and lower mantle (LM). The ppv transition has a minor effect on the dynamics and mantle temperature, mildly destabilizing the lower boundary layer (Tackley et al. 2007). However, the topology and dynamics of the seismically defined D" layer at the bottom of the mantle are controlled by the ppv transition (Monnereau and Yuen 2007). When compositional effects on the stability of ppv are taken into account, a large potential variety of complex behaviour could occur, generating structures such as discontinuities, gaps or holes and multiple crossings. The different contributions to seismic heterogeneity have different spectral slopes: temperature is long-wavelength, composition is 'white' and ppv is intermediate (Tackley et al. 2007).

Table 1 Mean parameters of the main phase transitions in the Earth's mantle, based on Schubert et al. (2001) for the first two transitions and on Hirose (2006) for the postperovskite transition. The affected mantle proportion, c, is based on a pyrolite composition. $\Gamma = \mathrm{D}p/\mathrm{D}T$ is the Clapeyron slope, ol – olivine, pv – perovskite, ppv – postperovskite

	Mean depth [km]	Width of the two-phase zone [km]	Γ [MPa/K]	$\Delta\rho/\rho$	c
ol → β-sp	410	10–20	1.6	0.070	0.58
γ-sp → pv	660	4–7	–2.5	0.100	0.58
pv → ppv	2600	30–35	8.0	0.011	0.72

The above transition depths are for mean mantle temperatures. In fact they occur over some depth range, depending on temperature variations due to convection. However, e.g. topography of the phase boundary around 660 km depth is less than 50 km. Hence it cannot be resolved directly in large scale models. We use a parameterization for the three dynamic effects of all considered phase boundaries.

The first effect is additional buoyancy in the momentum Eq. (5), due to the phase boundary distortion by advection of thermal anomalies. This buoyancy is,

$$F_B = \Gamma \cdot \frac{\Delta\rho}{\rho} \cdot A \cdot \Delta T \tag{14}$$

over a phase boundary area A, which has a temperature difference ΔT with respect to the mean temperature at that depth. $\Delta\rho$ is the density difference of the advected anomaly with respect to the surrounding density ρ. We neglect the possible temperature dependence of Γ (Hirose 2002).

The second effect is the release or absorption of latent heat, E_{latent}, which distorts the phase boundary by changing the temperature. We calculate the latent heat from the Clausius-Clapeyron formula,

$$E_{latent} = \Gamma \cdot \Delta V \cdot T \tag{15}$$

with $\Delta V \approx V \cdot \Delta\rho / \rho$ and the processed volume $V = v_r \cdot \Delta t \cdot A \cdot c$, during time step Δt, over area A, having a mean vertical velocity v_r, affected mantle proportion, c. The rate of latent heat production,

$$H_{latent} = E_{latent} \,/\, \rho V \Delta t \tag{16}$$

is added to the energy Eq. (6), but only at the grid layers next to the phase boundaries, with appropriate weighting. The work due to volume change at the phase transition, $p\Delta V$ is reflected in the density profile and therefore automatically accounted for in the energy Eq. (6).

The third effect is the expansion or contraction due to the release or absorption of latent heat. It is automatically accounted for via the temperature field, like any other thermal buoyancy.

3.1.3 Geochemistry – a Primer

Radiogenic *trace elements* in the mantle record differentiation events that change the parent/daughter ratio. The subsequent decay in isolated reservoirs allows dating of the differentiation event, if the decay time constant is in a matching order of magnitude.

The existence of geochemically distinct reservoirs in the Earth's mantle is inferred from the observation of worldwide rather homogeneous mid-ocean ridge basalts (MORB) on the one hand and heterogeneous ocean

island basalts (OIB) on the other (Hofmann 1997). Of course, what we observe today is the result of the interplay between chemical differentiation and convective stirring that started with the formation of the Earth and is still going on.

Seismic tomography provides a snapshot of the modern mantle. Wave speed anomalies are interpreted as evidence for subducting slabs that extend from the surface to the lower or lowermost mantle (Grand et al. 1997), (Trampert et al. 2004) and for superplume upwellings from the core mantle boundary (CMB) region (Su et al. 1994; Ritsema et al. 1999; Ritsema and van Heijst 2000). Together with the prevailing surface plate velocities these seismic observations lead most investigators to conclude there has been considerable mass exchange between upper and lower layers of the mantle for at least the last 100 Ma.

The reconciliation of geochemical and geophysical evidence has long been an unresolved problem in geodynamics. How can different geochemical reservoirs be maintained in the presence of large-scale convection for a long time? Why is one part of the mantle more homogeneous on a global scale than other parts?

3.1.4 Geochemical Heterogeneities

The size of observed geochemical heterogeneities ranges from cm-scale structures in high-temperature peridotites (Allègre and Turcotte 1986) to the DUPAL anomaly (Hart 1984). The latter seems to have a different origin in the Pacific than in the southern Atlantic and Indian Ocean (Hanan et al. 2004), so it is not global. Yet its existence for at least 115 Ma (Weiss et al. 1989) indicates that there is limited large-scale lateral stirring somewhere in the mantle.

The OIB isotopic compositions are far more diverse than MORB compositions (Allègre 2002), with the global variance of isotopic ratios for OIB being three times larger than the corresponding global variance of MORB (Allègre et al. 1987). The degree to which mantle heterogeneities are reflected in the resulting basalt depends on the degree of partial melting, magma mixing and extraction, the size of the volume that is sampled by partial melt, and the dimension of geochemical heterogeneity itself. Differences in composition and heterogeneity between OIB and MORB could be due to different sampling processes (Meibom and Anderson 2003), sampling of different geochemical reservoirs (Hofmann 1997) or a combination of these (Kellogg et al. 2002). The concept of a reservoir is here used to reflect a scale of systematic variation of mantle geochemistry that is too large to be erased by the sampling process. Sampling at mid-ocean ridges, for instance, acts on a scale of 30–200 km in depth and

several 100 km in width (Presnall et al. 2002) and hence the scale of the implied reservoir is larger.

3.1.5 Mantle Degassing

From the amount of ^{40}Ar in the atmosphere it has been estimated, that only about 50% of this isotope have been degassed from the mantle (Allègre et al. 1996). The low concentration in MORB suggests there is another reservoir containing the missing ^{40}Ar. This is a strong argument against simple whole-mantle convection (Hofmann 1997). However, it is subject to challenge, because the amount of ^{40}K (exclusively producing ^{40}Ar) in the Earth (Coltice and Ricard 2002), the efficiency of Ar degassing (Watson et al. 2007) and the role of Ar recycling (Rüpke et al. 2003) are poorly constrained. Seawater recycling might actually control the argon chemistry of the mantle (Holland and Ballentine 2006).

Nearly all the ^{3}He coming from the mantle is likely to be primordial, supporting the conclusion that the Earth has never been completely degassed (Gonnermann and Mukhopadhyay 2007). The ratio ^{3}He/^{4}He is very uniform in MORB, but varies in OIB. There could be a reservoir of absolutely high ^{3}He concentration, possibly 3.5 times higher than currently estimated from He flux (Ballentine et al. 2002), possibly poorly degassed or primordial mantle. High ^{3}He/^{4}He signatures might also originate in recycled material, if He degassing near the surface is less efficient than extraction of ^{4}He producing U and Th (Watson et al. 2007), or if recycled material is convectively isolated for long enough (Ferrachat and Ricard 2001).

3.1.6 Interpretation of Reservoirs

The MORB source region is sampled by the network of divergent margins all over the world and therefore is thought to occupy the shallow mantle (Hofmann 1997). The fixity of OIB-producing hot spots relative to surface plate movements is a compelling indicator that these plumes originate in and sample deeper regions of the mantle that are more or less decoupled from the surface motion. This is independently supported by tomographic images of deep-rooted plumes under OIB hot spots (Montelli et al. 2004), but hard to reconcile with a proposed (Meibom and Anderson 2003) shallow origin for all geochemical heterogeneity.

The roughly complementary geochemical signatures of CC and MORB are interpreted to be the result of primary extraction of CC from the original, primitive mantle (PM) (Hofmann 1988) or from an early depleted reservoir (EDR) that had already lost incompatible elements to a sunken enriched reservoir (early enriched reservoir – EER) (Boyet and Carlson 2005).

Mixing of all OIB would not give MORB. Other reservoirs proposed to contribute to OIB in differing proportions are EM1, EM2 (enriched mantle) and HIMU (high $\mu = {}^{238}\mathrm{U}/{}^{204}\mathrm{Pb}$). HIMU could be subducted oceanic crust, EM1 delaminated lower CC (Hofmann 1997) or subducted oceanic plateaus (Albarède 2001) and EM2 subducted continental sediments. The MORB source (depleted MORB mantle, DMM) is variably polluted on a regional scale by other components (Hanan et al. 2004). However, the absence of PM samples does not preclude the existence of a primitive reservoir (Kellogg et al. 2002).

3.1.7 Age of Reservoirs

The mean age of CC is 2–2.5 Ga, and that of oceanic basalts 1–1.3 Ga (Hofmann 1997). However, that is not necessarily the age of original differentiation (Albarède 2001). The depleted signature of MORB may (partly) reflect differentiation in a terrestrial magma ocean, 4.53 Ga ago (Boyet and Carlson 2005). The oldest HIMU signature is about 2 Ga (Hofmann 1997). Not introducing HIMU into the mantle prior to 2–2.5 Ga before present, due to a change in the surface oxidization environment or to subduction zone processes, could explain that age (Xie and Tackley 2004). The coincidence with the assumed end of primary CC segregation is striking.

3.1.8 Size of Reservoirs

How much of the mantle must have been depleted in incompatible elements to form the present volume of CC? Estimates depend on the geochemical models used and range from 25 to 90% (Hofmann 1997), but more likely 40–50% (Allègre 2002) – if CC was extracted from a primitive reservoir. If there was an early differentiation event (into EDR and EER) or if the bulk composition of the earth is different to primitive chondritic meteorites, then roughly 96% of the mantle must be as incompatible element depleted as the MORB source (Boyet and Carlson 2005) (Carlson et al. 2007). There must be one or more reservoir(s) containing the missing elements, in particular, the heat-producing nuclides ($^{235}\mathrm{U}$, $^{238}\mathrm{U}$, $^{40}\mathrm{K}$, $^{232}\mathrm{Th}$) and $^{40}\mathrm{Ar}$ (Albarède and van der Hilst 2002).

3.1.9 Reconciliation of Geophysical and Geochemical Constraints

There are several proposals how the depleted, well-mixed DMM could be separated from the other reservoirs and evolve independently for billions of years.

Phase boundaries: The γ-spinel-to-perovskite-plus-magnesiowüstite phase transition at 660 km depth hinders convection. It is appealing from a geochemical point of view to assume that it forces the upper mantle to convect separately from the lower mantle, but results of seismic tomography (e.g. van der Hilst et al. (1997), Trampert et al. (2004)) show penetration of the boundary today. On the other hand, temporal layering has been proposed on geological (e.g. (Condie 1997), geophysical (Breuer and Spohn 1995) and geochemical (Hofmann 1997; Allègre 2002) grounds. The necessary change in the effect of the phase transition could be due to the temperature-dependence of the Clapeyron slope (Hirose 2002) or the decreasing Rayleigh number (Ra) of the Earth (e.g. Tackley (1996)). However, at the Ra range assumed for the Earth, dynamic models commonly show avalanches through the phase boundary rather than long-term layering (Tackley 1996).

Small-scale heterogeneities plus D": The assumption that large-scale convection implies very efficient stirring leads to a cartoon with nearly the entire mantle being homogeneous DMM. Only D" remains as a possible repository of enriched reservoirs and hence as the OIB source region (e.g. Stegman et al. (2002)). OIB plumes originating at shallower depths (Montelli et al. 2004) are an argument against this model. Additionally, D" is a rather small volume in which to fit all the heterogeneities (Hofmann 1997; Albarède and van der Hilst 2002). On the other hand, by assuming that the 'homogeneous' mantle is riddled with small scale (~8 km: (Helffrich and Wood 2001)) up to regional scale (~100 km: (Meibom and Anderson 2003)) blobs of recycled material, the model becomes geochemically more plausible. Coltice and Ricard (2002) suggest a marble-cake mantle with recycled OC and peridotites containing primitive veins. In this case the mantle is assumed merely to be better mixed within the MORB source region than below it. Differing geochemical signatures are formed by mixing different amounts of these components, and because of segregation of dense OC, possibly in D". Heterogeneities smaller or comparable to the scale of sampling are supported by observations, but larger scale heterogeneities also exist (Trampert et al. 2004). None of above models, however, conclusively explains the coexistence of a shallow, more homogeneous reservoir and a deeper, less mixed one.

Different intrinsic densities: The nature of the D" layer is not entirely clear yet. It might be dominated by the effects of the perovskite to post-perovskite phase transition (Monnereau and Yuen 2007), or higher internal density (Nakagawa and Tackley 2004). If the compositional part of D" is due to subducted OC (eclogite), it could be the HIMU reservoir (Hofmann 1997). If it is foundered early crust (Tolstikhin and Hofmann 2005), D" could serve as a source for primordial gases and missing incompatible elements.

A similar proposal of early differentiation suggests that incompatible elements became enriched in a late crystallising layer of the terrestrial magma ocean – near the surface of the Earth. The residual of a magma ocean solidifies into a heavy layer that may sink, dragging the early enriched reservoir to the bottom of the mantle. There it could remain unsampled and undetected until today. Such a scenario might explain that primitive meteorites – believed to be the building blocks of the Earth – have a slightly skewed isotopic composition with respect to mantle samples (Boyet and Carlson 2005; Carlson et al. 2007). However, the solar nebula – from which the Earth and meteorites formed – was isotopically heterogeneous in the first place (Andreasen and Sharma 2006; Ranen and Jacobsen 2006). This could also explain the differences between chondritic meteorites and the Earth, supported by the fact that the Moon has an isotopic signature similar to the Earth's mantle. The Moon likely formed from a giant impact into the Earth's mantle, but simulations suggest that at least two-thirds of the material that makes up the Moon derived from the impactor, not from Earth (Canup 2004). Either the impactor had a similar history of silicate differentiation as the early Earth or both formed from material that had a different isotopic signature to chondritic meteorites.

Alternatively, a stable layer of dense melt may have formed at the base of the mantle early in the Earth's history (Labrosse et al. 2007), possibly having a thickness of about 1000 km. Such an initial, basal magma ocean would have undergone slow fractional crystallization, and it would be an ideal candidate for an unsampled geochemical reservoir. It could host a variety of incompatible species (most notably the missing budget of heat-producing elements) and might also explain the geochemical observations of Boyet and Carlson (2005).

A stable dense layer at 1500–2000 km depth was put forward by Kellogg et al. (1999) and could represent a leftover feature from the mantle's early evolution, e.g., magma ocean crystallisation (Hofmann 1997). Its seismic invisibility combined with fluid-dynamical constraints, however, weighs against the presence of such a layer today (Oldham and Davies 2004).

Dense material near the CMB could also be swept into ‘piles’ beneath upwellings and thinned, possibly to zero, under downwellings (Tackley 2000). This model is consistent with seismic tomography (Tackley 2002; Trampert et al. 2004), but the volume of the piles is still rather small to satisfy geochemical constraints (Hofmann 1997). It is not known whether dense piles can be formed and maintained by modern tectonic processes at the surface, or by core-mantle interactions, or represent a leftover expression of magma ocean fractional crystallisation, or a combination of these van der Hilst (2004).

Viscosity contrasts: Blobs having a 10–100 times higher viscosity resist stretching and mixing by the surrounding mantle (Manga 1996). It is conceivable, that 35–65% of the mantle could consist of such PM blobs and be concentrated in the LM (Becker et al. 1999). The lack of sampling of any such PM components at mid-ocean ridges and their need for persisting negative or neutral buoyancy despite substantial heating internal to the blobs are arguments against the model.

Other studies focus on radial viscosity stratification. Neither sufficient layering in the stirring efficiency (Stegman et al. 2002) nor significant convective isolation (van Keken and Ballentine 1998), (van Keken and Zhong 1999), (Ferrachat and Ricard 2001) were found for moderate viscosity contrasts. A model with more extreme contrasts (> factor of 1000) developed small-scale dominated whole mantle convection and separate reservoirs for DMM and PM, but no deep subduction (Walzer and Hendel 1999).

Allègre (2002) surmises that vigorous convection in the asthenosphere and sluggish stirring in the high viscosity transition layer both contribute to maintaining the MORB source region.

Filtering in the transition zone: The solubility of water above the β-to-γ-spinel transition is smaller than in the transition zone beneath it. Water lost from rising material lowers the melting temperature, possibly leading to a thin layer of partial melt at 410 km depth. Melt at that depth is denser than the matrix and will not rise. Incompatible elements concentrate in the melt and therefore only depleted material would reach the shallow mantle (Bercovici and Karato 2003). This hypothised filtering mechanism must be less efficient in hotter environments, allowing OIB forming plumes to retain enriched signatures. The temperature dependence would also allow CC to be formed from a volume larger than that above the transition zone.

3.2 Model Setup

Our convection calculations in this case study are restricted to uniform chemical composition and only consider the phase boundaries at 410 and 660 km depth. Thermal conductivity is constant in all models: $k = 12\ \mathrm{Wm^{-1}K^{-1}}$. Radial profiles for p_r, ρ_r, g, K_T were taken from PREM (Dziewonski and Anderson 1981), for c_V (Fig. 1a) and γ (Fig. 1b) were derived by (Walzer et al. 2003; 2004a) based on PREM. α is shown in Fig. 1d, T_r in Fig. 3a. Lateral variations of ρ are allowed according to Eq. (7).

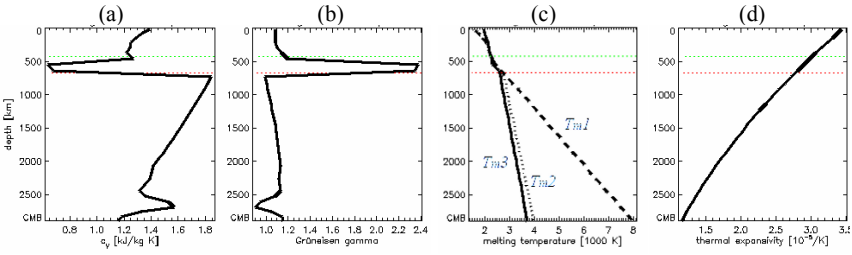

Fig. 1 All models feature these radial profiles of (**a**) specific heat at constant volume, (**b**) Grüneisen parameter, (**c**) melting temperature T_m1, T_m2, T_m3 and (**d**) thermal expansivity

We use three different profiles for the melting temperature T_m (T_m1, T_m2, T_m3) (Fig. 1c). In T_m1 (Walzer et al. 2003) the melting temperature is linearly interpolated between 660 km depth and CMB, according to experimental results of (Zerr and Boehler 1993; 1994). In T_m2 the melting temperature at the CMB was adjusted to results of (Boehler 2000). T_m3 is taken from Walzer et al. (2004a).

The heat generation rate per unit volume due to the decay of ^{40}K, ^{242}Th, ^{235}U, ^{238}U in the models is spatially homogeneous, but decays exponentially with time. Parameters are based on Walzer et al. (2004a). The observed scale of plumes (Montelli et al. 2004) is on the order of our grid resolution and their existence depends on the strong lateral temperature dependence of viscosity. Therefore, a self-consistent formation of small-scale plumes is not possible in our models. On the other hand, major partial melting is expected only near the surface, possibly above the CMB and near 410 km depth. In order to prevent unrealistically high temperatures, we considered cooling due to volcanism and small-scale plumes in the energy equation of some models. It is active only where $T > T_m$ and can be restricted to certain depths and basically means cutting $T > T_m$ to $T = T_m$ each time step:

$$\rho \cdot H_{cool} = \rho \cdot c_v \cdot \frac{d(T - T_m)}{dt} \tag{17}$$

3.2.1 Rheology

There is a low viscosity asthenosphere beneath the lithosphere and there are layers of higher viscosity beneath the asthenosphere. Otherwise there is currently no consensus on the laterally averaged viscosity profile of the Earth's mantle. In particular it is not clear if there is another low-viscosity zone near the boundary between upper and lower mantle or if the viscosity just increases there. However, the endothermic phase transition that separates the upper from the lower mantle, acts as dynamic barrier and is a net hindrance to vertical mantle flow. The bulk viscosity of the lower mantle is about 100 times higher than in the upper mantle.

Here we use Newtonian rheology with an Arrhenius law (Eq. (11)), $\xi = 17$ (Karato et al. 2001) and $\eta_0 = 10^{21}$ Pa s. The radial variation of $\eta(T)$ has been included in a profile $\eta_r(r)$, which also accounts for pressure dependence and compositional effects in the real Earth. For numerical reasons the lateral variability had to be damped by a factor c_t, which does depend on radius (Fig. 2a) in some models and is constant in others.

$$\eta(r,\theta,\varphi,t) = \eta_r(r) \cdot \exp\left[c_t(r) \cdot T_m(r) \cdot \left(\frac{1}{T(r,\theta,\varphi,t)} - \frac{1}{T_{av}(r,t)} \right) \right] \tag{18}$$

Viscoplastic yielding (Eq. (13)) is considered in the uppermost 285 km of the mantle. This weakening is not affected by c_t, but limited to $\eta_{eff} \geq 0.002 \cdot \eta$.

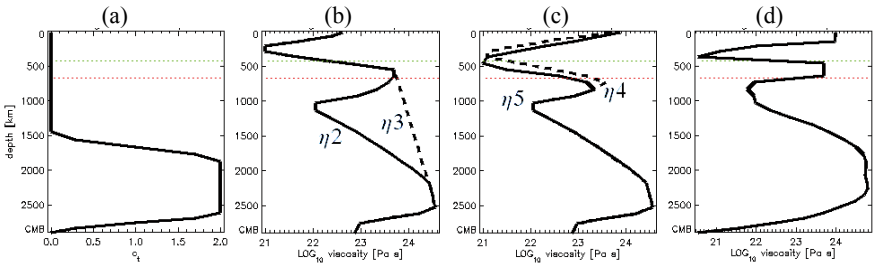

Fig. 2 (**a**) Radial variation c_t1 of the numerical damping factor, if not constant, (**b**) viscosity profiles $\eta 2$ and $\eta 3$, (**c**) viscosity profiles $\eta 4$ and $\eta 5$, (**d**) viscosity profile $\eta 6$. (**a**) and (**b**) are based on Walzer et al. (2003) and (**d**) on Walzer et al. (2004a)

We use different radial profiles $\eta_r(r) = \eta\#$ (Figs. 2b, c, d). The simplest case, $\eta 1$, is a constant viscosity of 10^{23} Pa s throughout the mantle. $\eta 6$ and $T_m 3$ are favoured for the modern mantle and were derived (Walzer et al. 2004b) from PREM by using solid-state physics considerations, thermodynamic relations, the Grüneisen parameter and Lindemann's law. The profile is anchored at 10^{21} Pas in the asthenosphere. That value is higher than assumed for the Earth (Dixon et al. 2004), but reflects our present numerical capabilities. $\eta 2$ is an earlier version (Walzer et al. 2003) of $\eta 6$, with a weaker lithosphere and smoother gradients. Physically more desirable steep gradients were taken out there for numerical reasons. A non-conventional feature of $\eta 2$ is a second asthenosphere below the transition zone. This weak layer is omitted in $\eta 3$ in order to test its influence on the convection. When applied to models using $\eta 2$, the module based on (Eq. (13)) had virtually no effect. Therefore $\eta 4$ and $\eta 5$ were introduced, featuring stiffer lithospheres but still keeping gradients smooth. Both are generally weaker than $\eta 6$ and can therefore be interpreted to show effects of a supposedly hotter, early mantle. However, no attempt has been made here to address shape and amplitude of the viscosity profile for the Archean mantle. We stress that profiles based on PREM are valid for the modern mantle only and that our present models do not include time dependence in the assumed radial viscosity profile.

3.2.2 Boundary Conditions

The computing domain is a thick spherical shell, mimicking the silicate part of the Earth. The inner boundary at r_{CMB} = 3480 km and the outer boundary at r_E = 6371 km are free of tangential stresses, because the viscosities of liquid outer core and atmosphere/hydrosphere are negligible compared to mantle rocks.

A constant temperature of 288 K is assumed for the outer boundary, because it is the mean surface temperature today and there has been liquid water on the surface for at least 3.8 Ga.

Different thermal boundary conditions at the CMB reflect the continuous development of our models rather than being a focus of this paper. Condition *CMB*1 means a heat flux of 28.9 mW m^{-2} (Anderson 1998), temporally (Schubert et al. 2001) and laterally (Walzer et al. 2003) constant. This was changed to spatially constant temperature, which is adjusted every time step to ensure a mean heat flux constant in time (*CMB*2). The physically most appealing approach is to couple a parameterised model of the evolution of the core to mantle convection. The heat flux across the CMB is equalled by secular cooling of inner and outer core, latent heat from freezing or melting of the inner core, release of gravitational

potential energy due to the preferred segregation of heavy elements at the inner core boundary and the radiogenic heat production of the core. This energy balance was calculated every time step to obtain heat flux and spatially constant temperature at the CMB as well as the radius of the inner core. The core model is based on Labrosse (2003) and the implementation is described in detail by Gottschaldt (2003). This kind of boundary condition is characterised in the following by the concentration of ^{40}K, which is thought to be the major radiogenic heat source in the core.

3.2.3 Initial Conditions

Because of the assumption of infinite Prandtl number and homogeneous composition, we need to consider only the initial temperature field. The thermal state of the early Earth is highly speculative, and we have explored several different scenarios. Frequent impacts may have determined the heat structure of the outer layers (Arrhenius and Lepland 2000), leading to an early thermally stable stratification. A global magma ocean (Solomatov 2000) or several large scale melting events (Kleine et al. 2004) are also conceivable. Fractional crystallisation and subsequent overturn has the potential to result in compositionally or thermally stable layering, too (Elkins-Tanton et al. 2003; Zaranek and Parmentier 2004). In this context we used a starting profile of constant temperature $T_{av}(r)$, which is stable in a compressible mantle. Only in the upper boundary layer did we introduce a smooth transition to the surface temperature (Fig. 3b). Together with a small lateral perturbation of the form

$$T(r,\theta,\varphi) = T_{av}(r) + T(\theta,\varphi)\cdot\cos\left[\frac{\pi}{r_E - r_{CMB}}\cdot\left(r - \frac{r_E + r_{CMB}}{2}\right)\right] \tag{19}$$

with

$$T(\theta,\varphi) = \sum_{l=2}^{15}\sum_{m=1}^{l} 0{,}002\cdot(-1)^m \cdot P_l^m(\cos\theta)\cdot\left[\cos(m\varphi) - \sin(m\varphi)\right] \tag{20}$$

this initial condition is called *IC*1. P_1^m is a Legendre function. The above perturbation is used for all models of this study. In *IC*2 a lower thermal boundary layer was added (Fig. 3c). An adiabatic profile plus boundary layers (Stacey 1992) and the solidus T_m3 are more obvious starting profiles, used in *IC*3 (Fig. 3d) and *IC*4 respectively.

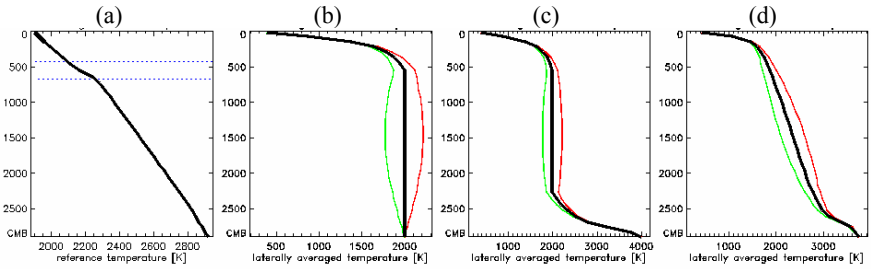

Fig. 3 Radial profiles of (**a**) reference temperature T_r, (**b**) initial temperature (*black*) and maximum perturbation (*grey*) for *IC1*, (**c**) *IC2* and (**d**) *IC3*. *Dotted lines* in figure (**a**) mark the phase boundaries, which are considered in the code

3.3 Numerics

3.3.1 Mantle Convection Code: TERRA

The coupled system of equations is solved numerically with the well-established Fortran code TERRA (Baumgardner 1983; Yang 1997) for the whole evolution of the entire mantle. The computational grid is based on a projection of the regular icosahedron onto a sphere and successive dyadic refinements (Baumgardner and Frederickson 1985). Concentric copies of such spherical layers of nodes build the domain in radial direction. All models have been run on a grid with 1394250 grid points, corresponding to a spatial resolution on the order of 100 km. Equations (2) and (4) are discretised in an Eulerian approach by finite elements with linear basis functions and solved simultaneously (modified after Ramage and Walthan (1992)) using a multigrid method. The energy equation is discretised by the MPDAT algorithm (Smolarkiewicz 1984) and integrated with a Runge-Kutta scheme using explicit time stepping. Domain decomposition is used for the parallelisation (Bunge and Baumgardner 1995) with MPI. TERRA was benchmarked for constant viscosity convection by Bunge et al. (1997) with numerical results of Glatzmaier (1988) for Nusselt numbers, peak temperatures, and peak velocities. A good agreement ($\leq 1.5\%$) was found. However, strong viscosity variations challenge the stability of the code and results should be interpreted as approximations. No detailed error analysis (DeVolder et al. 2002) was done.

3.3.2 Treatment of Compositional Fields

There are several methods to approximate the advection of non-diffusive scalar fields in thermal convection (van Keken et al. 1997). We use passive Lagrangian tracers that have no feedback on convection. Since the focus of this study is on large scale stirring, it was sufficient to initialise only two tracers per grid point. More tracers would be necessary for modelling chemical differentiation with active tracers, reproducing local geological features or characterise mixing across different scales. For testing, case H was repeated, starting with eight tracers per grid point. Without fine tuning nearly every second tracer was lost during the run, still giving twice the standard resolution at the last time step. A spherical harmonic analysis of the chemical field reveals not much structure above degree 30, so we cut it off there. The relevant results (Figs. 4, 5) are basically identical to the low resolution run.

Each tracer represents half of the mass of its initial cell and keeps this attribute throughout the entire run. Trajectories of the tracers are calculated synchronous to the integration of the heat equation. They move independently of the TERRA grid, but are continuously re-indexed with respect to the nearest grid point. This allows efficient interpolation between the Lagrangian particles and the local neighbourhood of Eulerian grid points. Memory requirements limit the number of tracers that can be hosted by a single grid point. If a grid point becomes overcrowded, surplus tracers are deleted randomly. With ~2% lost tracers and ~5% empty cells after a typical evolution run coverage is reasonably good. The accuracy of tracer trajectories was tested with prescribed velocity fields. Deviations from the analytic solution were less than 0.006%, which means ~10 km for a typical run.

3.3.3 Definition of Two Components

Here we want to track the dispersion of the material that comes close to the surface (‘degasses’) and characterise its subsequent distribution in the mantle at discrete time steps. In this framework we shall define two components, degassed tracers and residuum, and apply two constraints in our definition:

1. Each component will comprise 50% of the mantle at the end of the convection calculation. This ensures the comparability of different models. The half-half distribution is the most sensitive for measuring the state of stirring between two components.
2. It must represent a reasonable approximation for chemical differentiation near the surface. This corresponds to the fact that major differentiation

processes like the extraction of CC and degassing are related to partial melting near the Earth's surface. Hence the term 'degassing' is used here for a range of chemical modifications near the surface.

The following algorithm is used to satisfy both constraints: No compositional information is assigned to tracers during the convection calculation, but each tracer remembers its closest approach to the surface. This information is output together with the Cartesian coordinates and the mass of each tracer. In postprocessing, the tracers are ordered according to that distance, starting with the smallest. Then their masses are added successively until the sum has reached 50% of the mantle mass. The distance attribute of the last tracer incrementing this sum is taken as degassing depth (d_d). In other words, the degassing depth is an output, not an input. All tracers which have been closer to the surface than the degassing depth are assigned the concentration $c = 0$, while the residuum retains a concentration $c = 1$. This is identical to ongoing differentiation throughout the run with complete degassing above and none below the degassing depth. The algorithm describes modification of pristine mantle near the surface and degassing of primordial, non-radiogenic gases. It is not necessary to prescribe degassing locations such as mid-ocean ridges or volcanoes, because mantle rock can reach the surface only at these locations. The concentration of undegassed material in each grid cell is the mean of the concentrations of all the tracers it contains, weighted by their masses.

3.4 Model Results

The ultimate goal of convection-differentiation models is to reproduce observations. For geochemistry this would be plots of isotopic concentrations in surface samples. Since no isotopic systems are modelled, this is not possible here. We focus on large-scale geometrical characteristics of the convective flow instead. For easy comparison, results are grouped together here and will be discussed in the next section. The parameter space covered by this study and some output values are summarized in Table 2. Maximum and root mean square (rms) surface velocity may be used to compare the convective vigour of our models to the Earth.

Table 2 Summary of models contributing to this study. Rheology is determined by the viscosity profile, denoted in column η, the numerical damping factor c_t and the yield stress τ_y. The melting temperature profile, volcanism model, boundary condition at the CMB and initial condition are given in columns T_m, *vol*, *CMB*, and *IC* respectively. τ_y is given in [10^8 Pa] and the concentration of ^{40}K in the core in column *CMB* in [ppm]. The results for root mean square velocity (v_{rms}) and maximum (v_{max}) surface velocity are in [cm/year], the degassing depth d_d is in [km]. All are for the last time-step

Model	η	c_t	τ_y	T_m	vol	CMB	IC	v_{rms}	v_{max}	d_d
A	η1	c_t1	–	T_m1	–	CMB1	IC1	0.2	0.7	144
B	η2	c_t1	–	T_m1	–			1.5	2.7	64
C	η2	c_t1	–	T_m1	–		IC3	1.4	2.5	62
D	η2	c_t1	–	T_m1	–	100	IC2	1.6	2.6	67
E	η2	c_t1	–	T_m1	–	200	IC2	1.7	2.9	66
F	η3	c_t1	–	T_m1	–	CMB1	IC1	1.7	2.6	69
G	η4	1.0	1.8	T_m1	vol1	CMB1	IC1	1.2	1.8	99
H	η5	1.0	1.8	T_m1	vol1	CMB1	IC1	0.5	1.4	163
I	η5	1.0	1.4	T_m1	vol1	CMB1	IC1	0.6	1.7	152
J	η5	1.5	1.35	T_m3	vol2		IC4	0.7	1.4	148
K	η6	1.0	1.4	T_m1	vol1		IC1	1.2	2.8	223
L	η6	1.0	1.35	T_m1	–	200	IC2	0.8	1.9	176
M	η6	1.0	1.35	T_m1	–	200	IC3	0.9	2.0	155
N	η6	1.0	1.35	T_m1	–	CMB2	IC3	0.6	2.2	150
O	η6	1.0	1.35	T_m2	vol2	CMB2	IC3	0.8	1.7	151
P	η6	1.0	1.35	T_m2	vol2	200	IC3	0.8	2.4	160
Q	η6	1.75	1.35	T_m2	vol2	200	IC3	0.7	2.1	144
R	η6	1.5	1.35	T_m3	vol2	CMB2	IC4	0.7	1.8	158

Besides of Table 2, results are presented graphically in Figs. 4, 5 and in the Supplementary Material (available on accompanying DVD). Temperature evolution plots display the laterally averaged temperature profile versus time in a contour plot. Accordingly, degassing evolution plots are based on laterally averaged profiles of the concentration of pristine material. The scale of heterogeneity in the distribution of degassed material is determined by a spherical harmonic analysis. We applied the method used by Yang (1997) to the field of concentration minus the mean concentration at each radial level. The resulting spectral heterogeneity map is a contour plot of the rms amplitude of the scalar field at different depths for spherical harmonic degrees 0–30. The colour scale of each plot is given as percentage of the maximum value occurring in that plot for all degrees and depths. A spherical harmonic analysis is only done for the last time step, corresponding to the modern Earth. The planform of the radial velocity component at 65 and 2825 km depths is given for three time steps. Only each group of three pictures shares a colour scheme. Cutaway views of the mantle show the degassing field at the same time steps as the velocity planform pictures. All cutaway views use the same colour scheme (for more information Please see the accompanying DVD).

Since some parameter variations have only minor influences on the convective flow, pictures are just given for selected models.

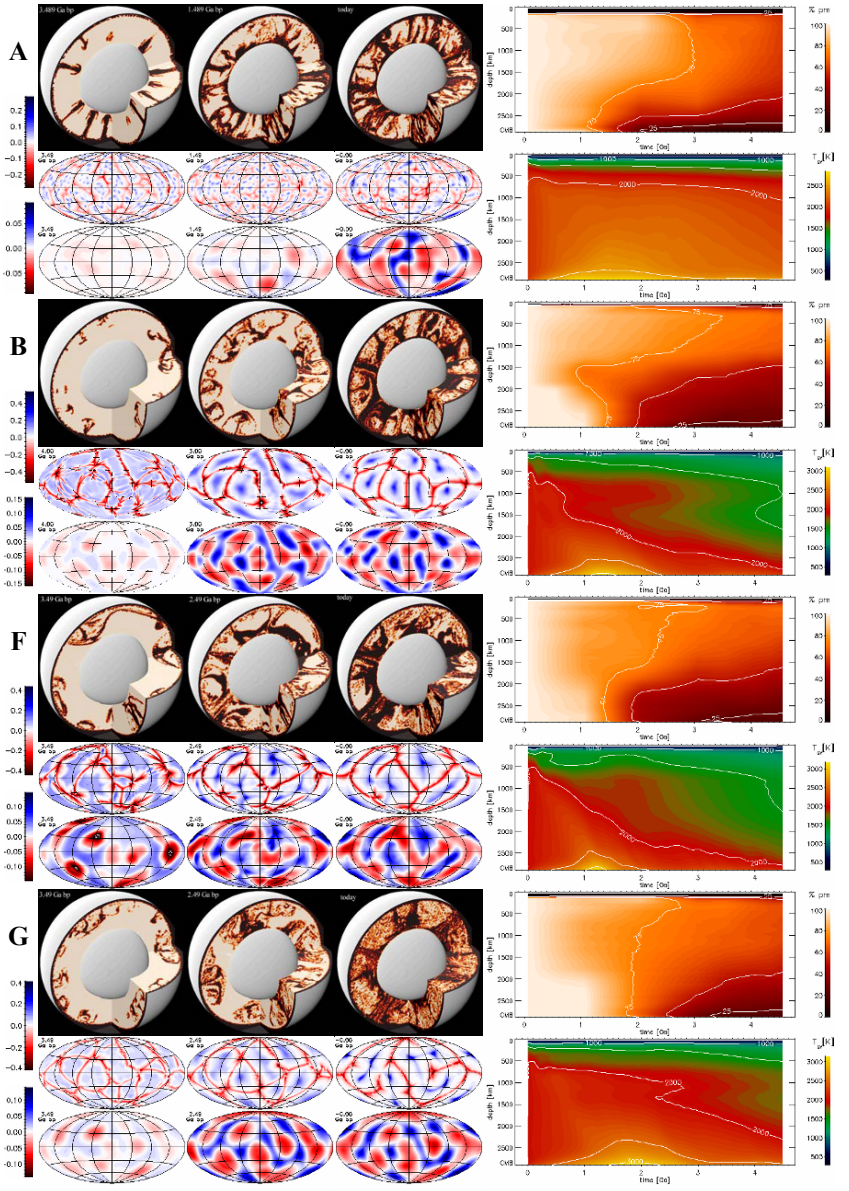

Fig. 4 Results of selected models. Three cutaway views of the mantle are placed to the *right* of the letter that is denoting the model. They show the degassing field at the same time steps as the planform of the radial velocity component is given below. The *upper row* always is for 65 km depth and the *lower row* is for 2825 km. Velocity is given in [cm a^{-1}] and each legend is valid for a *whole row*. Depicted

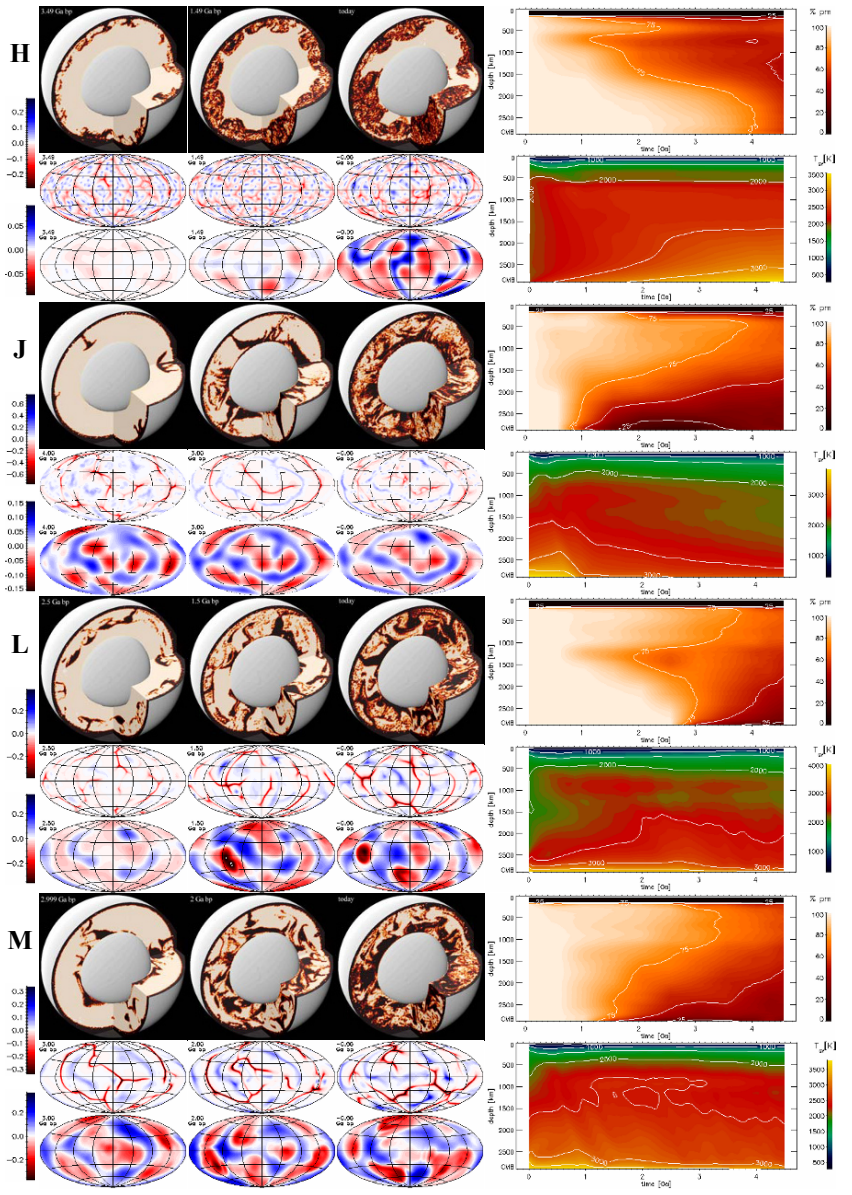

time steps were chosen separately for each model. Degassing evolution plot and temperature evolution plot are placed in the *right column*. *Light colours* in the degassing evolution plot indicate undegassed material (white = 100% pm). The legend is also valid for the cutaway views. Pictures of not displayed models (in *brackets*) are similar to: B ~ (C, D, E), H ~ (I), L ~ (K), M ~ (N, O, P, Q, R)

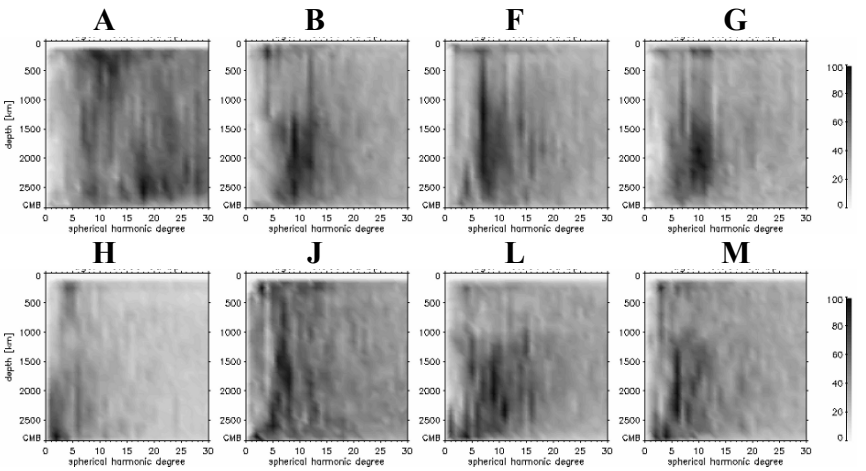

Fig. 5 Spectral heterogeneity maps for the distribution of degassed material in the last time step of selected models. The *grey scale* depicts the percentage of the maximum value occurring in each individual plot for all degrees and depths

The Supplementary Material contains additional visualizations of the evolution of the velocity fields for models A, F, C, I and K, as well as The Supplementary Material contains additional visualizations of the evolution of the velocity fields for models A, F, C, I and K, as well as animations of the degassing field for models A, C, I and K.

Animations of the degassing field for models A, C, I and K.

3.5 Discussion

Mean surface velocities in all models are smaller than the observed value of 3.9 cm a^{-1} (Gordon and Jurdy 1986) and the observed maximum velocities of more than 10 cm a^{-1} are not reached either. O'Connell et al. (1991) estimate that ~45% of the Earth's surface velocity field is in toroidal components, but our models all display less than 5%. Further shortcomings are discussed in Walzer et al. (2004b). However, currently there is no model of the Earth that satisfies all main constraints. The behaviour of the lithosphere at plate boundaries is determined by small-scale phenomena (fluids, melt, cracking and elasticity) that are not resolved in our global models. Besides a more realistic lateral variability of rheology, coupling between different scales is desirable in future models. Especially the outer boundary

needs improvement but the deep mantle could still be adequately represented here. We do not attempt to relate the timescale of our models to the real Earth. Despite the rather low convective vigour (measured by surface velocity), we find degassing depths between 62 and 258 km, which are in the same order of magnitude as concluded by other studies: 60–115 km (Hirth and Kohlstedt 1996), 65 km (Regenauer-Lieb and Kohl 2003) and the depth of partial melting (<200 km: (Presnall et al. 2002)).

3.5.1 Influence of Geometry

In model A, no radial viscosity variation is assumed. This is certainly unrealistic for the Earth, but most clearly demonstrates an effect of 3-d spherical geometry. Thermal convection in general is organised in cell-like structures, which may vary in their shape, symmetry, size and time dependence. Let's consider a single roll of constant angular velocity in an incompressible, isoviscous cube. There is a line of pure rotation through the centre of the roll, which lies at mid-depth in the cube. Conservation of mass requires that flux through a vertical plane below this stagnation line equals the flux through a plane above the line. Now let's shrink the bottom of the cube, making it a frustum of an upside down pyramid. The stagnation line will move upwards until the flux through the vertical plane above the line is the same as below. This is analogous to what happens in 3-d spherical geometry. The assumption of constant angular velocity is certainly not realistic and asymmetries in the velocity distribution of a cell will overlay the illustrated geometric effect. For example, the planform area of upwellings may be smaller or larger than that of downwellings, depending on the model and even depth. A detailed investigation of the implications and relative importance of these aspects is beyond the scope of this paper. In A degassed material from the top sinks right to the bottom of the mantle. There is only little hindrance at the depth of nonzero c_t, because viscosity is increased locally in cold downwellings. In lateral average degassed material fills the mantle from the bottom. The upper half of the mantle keeps its pristine signature for the longest time. This is due to the combined effects of cell geometry, flux asymmetry and lateral averaging. The latter just means that there is less volume in the LM for the same amount of degassed material than in the UM, giving LM a more degassed signature on average.

3.5.2 Influence of Rheology

Model B is identical to A except for the viscosity profile. Downwellings are hindered and partially deflected, when they hit the high viscosity zone

(HVZ) in the mid LM. This is evident in the first cutaway view and the high concentration of degassed material in about 1500 km depth during the first billion years of evolution. Furthermore the long-term preservation of pristine material in the upper half of the mantle is more pronounced than in A, with the lowest concentration of degassed material even closer to the surface. Velocities are lower in the HVZ of the lower mantle and consequently stagnation points of whole-mantle cells move further upwards. This effect is an additional reason for the more degassed signature of the LM. It has been observed in axisymmetrical models (van Keken et al. 2001) and even in Cartesian geometry (Ferrachat and Ricard 2001). A distinct concentration gradient at 1500 km depth is maintained after ~1.5 Ga. This suggests that there is some degree of decoupling. Cold material sinks efficiently into the HVZ and produces long-wavelength heterogeneity there due to sluggish stirring. On the other hand, ambient upwelling from the HVZ delivers an average, less degassed signature upwards. The planform of radial velocity shows that the area of up- and downwellings is about equal in the HVZ but in the UM downwellings are narrow.

This is also true for the planform of model F, where the lower low viscosity zone (LVZ) has been omitted. However, $l \sim 7$ heterogeneity is dominant throughout the mantle. This is a notable difference to B, where heterogeneity is pronounced in the HVZ. During its way down degassed material is stirred more efficiently, allowing only smooth concentration gradients in the lateral average. We conclude that the second asthenosphere is crucial for the decoupling of the stirring behaviour in the mid mantle.

Support for that conclusion comes from model G, which features the lower LVZ but a stiffer lithosphere plus yielding. That variation hinders convection as indicated by lower surface velocities. In the first billion years degassed material is dispersed in the upper half of the mantle, similar to F. When the stable initial temperature profile is overcome, large cells fill the mantle from the bottom with degassed material. At the end, heterogeneity is pronounced in the HVZ. Hence the resulting layering of stirring behaviour is not an artefact of the early mode of dispersion in the model.

Compared to G, the viscosity profile for H and I has a slightly thicker and stiffer lithosphere. This minor change triggers a rather different evolution. During the first billion years convection is hindered by the phase boundary and viscosity increase in 660 km depth, combined with the effects of the stable initial temperature profile and the stiffer lithosphere. Small-scale cells develop which efficiently disperse degassed material in the upper mantle. After about 1.5 Ga the boundary between the vigorous convecting zone and pristine mantle moves down through the second LVZ until it reaches the HVZ of the lower mantle. While hindered there, degassed

material is effectively stirred in the upper half of the mantle. However, the band of less degassed material in the degassing evolution plot at 500 km depth extends to at least 3 Ga. A less visible band develops at 1000 km depth. This indicates, that there are still some cells confined to the UM. Other cells are operating between the two asthenospheres, with their stagnation points in the stiffer transition zone. Between 3 and 4 Ga the lower half of the mantle starts to convect and the system switches to long wavelength convection. Regions with persisting small-scale convection are dragged into the mantle by this catastrophic overturn. No stability analysis (e.g. like Turcotte and Schubert (2002), p. 270) has been carried out, but obviously that behaviour may be explained as follows. Small-scale convection efficiently cools the upper half of the mantle, but it is not able to penetrate into the HVZ, where longer wavelength perturbations are unstable. Further cooling of the upper half and heating of the lower half increases the Rayleigh number of the whole system, finally leading to the rise of the lower layer. The long wavelength of that rising layer is thereby overprinted on the entire mantle. Walzer and Hendel (1999) found a similar behaviour in a 2-d convection-differentiation model without stable initial stratification.

The different yield stresses in H and I have only a gradual influence.

Profile $\eta 6$ in the otherwise identical model K initially leads to medium scale cells in the upper half of the mantle. There is no significant layering at the high viscosity transition zone or the phase boundary at 660 km depth, but instead at the lower HVZ. Large-scale overturn takes over before the upper half of the mantle is well stirred. This difference from models H and I is possibly due to the longer wavelength of the initial convection in the upper half of the mantle.

Profiles $\eta 5$ and $\eta 6$ are compared again in models J and R, but with an unstable initial temperature profile. There is insignificant or no layering of convection now. In both models, degassed material sinks from the top to the CMB in large-scale cells from the beginning. As in B, stagnation points occur in the upper 1000 km of the mantle (pronounced in J) and heterogeneity is expressed mostly in the lower HVZ (pronounced in R).

3.5.3 Influence of Initial Conditions

The comparisons of H versus J and K versus R indicate, that stable initial layering is necessary to confine early convection to the upper layers of the mantle. This conclusion is supported by L versus M, which differ only in their initial temperature profiles. Layering on top of the lower HVZ is much weaker in M, which has an unstable initial profile. As demonstrated by A and B, stable initial layering is not sufficient to trigger

layered convection. Walzer et al. (2004b) find the small-scale convective regime also in 2-d models with unstable initial temperature profiles, but with larger viscosity differences in the UM.

3.5.4 Minor Influences

According to Eq. (18) a higher melting temperature acts like an increased lateral temperature dependence of viscosity (c_t) at a given depth, and the volcanism module (*vol**) simply removes unrealistic peak temperatures. It follows from N versus O, that this difference affects degassing and global thermal history only slightly.

The thermal boundary at the CMB could affect the temperature profile and therefore has the potential to alter the whole evolution. However, comparison of models with core evolution versus constant heat flux (M versus N and P versus O) shows no significant difference in their degassing histories. The same is also true for D versus E, which feature different concentrations of ^{40}K in the core. All models with core evolution develop higher CMB heat fluxes than assumed for the other models. This leads to steeper thermal boundaries at the bottom. A wider parameter space ought to be explored, especially for the influence of the CMB heat flow in models with stable initial layering.

3.6 Conclusions

Despite the deficiencies of our models the following conclusions are considered to be reasonably robust for Earth-like parameters:

1. During large-scale convection in 3-d spherical geometry with a highly viscous LM, the upper 1000 km of the mantle are least affected by material that was subject to differentiation near the surface.
2. Realistic radial viscosity variations – with two low viscosity zones in the upper half of the mantle and a highly viscous LM – result in a layering of the stirring behaviour.
3. Small-scale convection confined to the upper parts of the mantle is possible under certain conditions.
4. The convective regime may change from small-scale to large-scale convection.

The timescale in our models is unlikely to correspond to the real Earth, because surface velocities are smaller than observed, the viscosity profile does not evolve and we only speculate about the initial conditions.

3.6.1 Relevance for the Earth

We promote the following cartoon (Fig. 6) to be considered in the list of possible scenarios for the convection-differentiation history of the Earth.

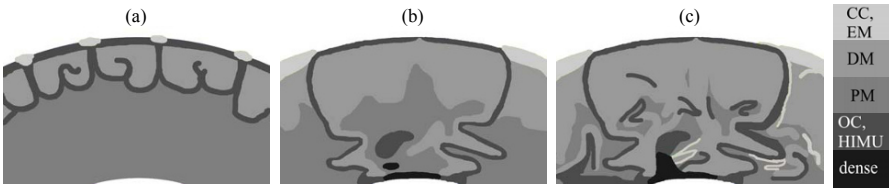

Fig. 6 During an episode of layered convection CC is extracted near the surface, leaving behind a depleted, well stirred residue above deeper pristine material (**a**) Later large-scale convection with deep subduction starts to work on this configuration (**b**) Further differentiation and segregation of CC takes place near the surface, but the shallow mantle is likely to retain its depleted, homogeneous signature due to 3-d spherical geometry and high viscosity in the mid lower mantle. Additionally, stirring is least effective in the mid lower mantle, allowing primitive and recycled material to coexist for the longest time in the convecting mantle. High density components may segregate in D". The modern MORB source would be a leftover from the episode of small-scale convection plus variable contamination from the lower half of the mantle. Small-scale plumes sampling different regions of the heterogeneous lower mantle produce the observed scatter in OIB geochemistry (**c**)

There may have been layered convection in the Archean mantle. CC is extracted near the surface and the residuum is well stirred by small-scale cells in the uppermost convecting layer, as in models H and I. A layer of homogeneous depleted material may grow on top of pristine mantle, as found in a convection-differentiation model of Walzer and Hendel (1999). The depleted layer is not necessarily confined to the UM and the boundary between both regions is irregular.

At some stage the system must have switched to the style of convection, which is favoured for the Earth today. There are downwellings plunging from the surface into the lower mantle or even to the CMB. Because of 3-d spherical geometry and high viscosity in the lower mantle the stagnation points of the cell-like convective structures lie at rather shallow depths. Additionally, broad up- and small downwellings would fill the mantle from the bottom with degassed material and rise old material that has been there before. Laterally averaged, material just below the depth of partial melting can preserve its original signature for the longest time. The original signature may be the depleted signature that is left from the episode of

small-scale convection. Stirring is less effective in the HVZ of the lower mantle and heterogeneities can persist there longer than in other parts of the mantle. Primordial material could have survived there, or, if stabilized by higher density, in D". Inefficient stirring in the HVZ also provides a mechanism to store recycled lithosphere (low U/He ratio) for some time. High $^{3}He/^{4}He$ signatures might arise there, due to retarded radiogenic in growth of ^{4}He, as suggested by Ferrachat and Ricard (2001). Toroidal components and plate velocities at the surface are larger in the real Earth than in our models. Therefore stirring of the MORB source is probably underestimated here and the heterogeneity contrast to the HVZ in the LM may be even larger in the real Earth. A filter operating in the transition zone (Bercovici and Karato 2003) is not essential in this scenario, but may help to maintain a homogeneous, depleted MORB reservoir.

Reasons for a change in the convective regime are speculative. The overcoming of initially stable layering – thermally or compositionally – might be a possibility. An impermeable boundary in the mid mantle is unlikely today, but compositional layering may have contributed to convective isolation of lower parts of the mantle in the early Earth. Layering is more sustainable with higher convective vigour (Davaille 1999; Oldham and Davies 2004). Therefore it is also likely that the phase boundaries (Tackley 1996) and steep viscosity gradients (Walzer and Hendel 1999) had a stronger layering effect in a more vigorous regime. Almost certainly the viscosity was generally lower in the Archean. Radiogenic heating has been steadily decreasing. Both effects support higher convective vigour in the early Earth and likely had the potential to change the convective style of the mantle. In our models the viscosity profile is fixed for each run, gradients are smoothed for numerical reasons and composition is uniform. Therefore layered convection in the Earth could have lasted longer than in the models – opposite to the effect of too small convective vigour on the model timescale. In the light of these competing shortcomings we cannot determine the duration of the layered period or the percentage of mantle processed from our models.

Additional feedback could come from spatially inhomogeneous radiogenic heating, with the pristine lower layer being heated more than the depleted layer. The proposed change in the style of subduction (Xie and Tackley 2004) could be contributing to or resulting from a change of the convective mode.

Two extreme scenarios are conceivable for the transition from small- to large-scale convection. One is the catastrophic overturn, captured in its initial stage by models H and I. The overturn is driven by the globally unstable layering and could result in a large-scale inversion of geochemical signatures, with pristine on top of degassed material. This is the opposite of

what is being concluded from OIB and MORB signatures (Ballentine et al. 2002). They also argue that this kind of overturn results in rising upper mantle temperatures, but this is not observed in the laterally averaged temperature profiles of H and I. The other scenario is more like that occurring in model G. Large-scale cells appear early, but are accompanied by small-scale cells. The small cells die out, leaving behind a well-stirred, depleted upper part of the mantle. Then large-scale convection takes over without catastrophic overturn. At some stage the existing long wavelength cells just start to penetrate the lowermost mantle. Local instabilities rather than unstable global layering control this onset of deep subduction. The second scenario is favoured here, but both are only a small change in lithospheric rheology apart (see discussion G versus H) and hence aspects of both may have been operating in the Earth. Neither mechanism has been investigated in detail as yet. Models G, H, and I show only certain aspects of each.

3.6.2 Other Hints for a Change of Convective Mode

A consequence of the scenario outlined above is that the upper parts of the mantle are heterogeneous in the early stages of small-scale convection and more homogeneous before the onset of large-scale convection. Large-scale convection increases heterogeneity again, leading to the modern geochemical scatter in mantle-derived rocks. Rare earth signatures in picrites and komatiites from the Late Archean are indeed more homogeneous than in samples from the Early Archean, Proterozoic and Phanerozoic respectively (Campbell 1998).

Breuer and Spohn (1995) propose a flush instability to explain geological and climate changes at the Archean-Proterozoic transition. There are several indications for rapid growth of CC, continents and ocean water mass during that time. CC growth is attributed to increasing UM temperatures, convective vigour and the lower mantle reservoir becoming available for CC extraction. Increased degassing of the mantle could lead to increased ocean water mass. This would be consistent with the catastrophic overturn scenario. Archean island-arc magmas originated in relatively warm, basaltic crust and at lower pressures than at present. This could be explained by a smaller plate scale (Taylor and McLennan 1995).

Based on supercontinent cycles and greenstone ages, Condie (1997), favours layered convection before 2.8 Ga bp, episodicity of catastrophic overturn and hindering of deep subduction until 1.3 Ga bp and large-scale convection afterwards. Allègre (2002) reviews geochemical constraints and concludes that they are consistent with layered convection earlier and large-scale convection today. Breuer and Spohn (1995), Condie (1997) and Allègre (2002) assume the phase boundary at 660 km depth leads to tem-

poral layering. However, their general arguments are also valid for the types of layering discussed here.

3.6.3 Outlook

Future models aiming at the reconciliation of geophysical and geochemical constraints may consider the following points:
(1) 3-d spherical geometry is important for global stirring.
(2) One or more changes of the convective mode during the evolution of the mantle are a possibility.
(3) Rheology has a strong influence on the stirring properties of the mantle. Shortcomings of our models are static viscosity profiles and an oversimplified lithospheric rheology that yields unrealistic (toroidal) velocities at the surface. Viscosity profiles should evolve according to the mantle temperature and more realistic lateral viscosity variations need to be included.
(4) Neither trace element nor major element compositional differences have been modelled here. A more direct comparison of models and observations would be possible by coupling the evolution of isotopic systems (like Xie and Tackley (2004)) or reservoirs (like Walzer and Hendel (1999), (2008)) to models of mantle convection. Inhomogeneous internal heating, different densities and viscosities could provide a feedback on thermal convection.
(5) We need a rational vision of Precambrian scenarios. Was there stable compositional or thermal layering? What was the tectonic style of the early Earth and how did chemical differentiation work, especially the segregation of CC?

As a working assumption we propose a marble cake like structure for the modern mantle, with small-scale geochemical structure dominating in the MORB source and heterogeneities larger than the sampling volume of deep-rooted plumes occurring in the LM. This includes segregation and temporal or permanent storage of dense recycled material above the CMB. The more homogeneous structure of the shallow mantle could be a leftover from an episode of small-scale convection and differentiation near the surface, combined with the effects of 3-d spherical geometry and the viscosity profile. Primitive material is most likely to have survived in the poorly mixed HVZ in the mid LM. It may reach the UM only as small-scale veins that are homogenised during sampling. A pure recycling model is also conceivable. The relative importance and time-dependence of additional mechanisms, like zoning by variable depth of subduction, a filter contributing to the homogeneity of DMM, differences during melt extraction and the statistical nature of sampling and the possibility of a doming regime

with dense piles in upwellings may be investigated in more sophisticated future models.

Acknowledgements The calculations for this paper were done on the supercomputers of the John-von-Neumann Institute for Computing at Forschungszentrum Jülich (Germany) and the Earth Systems Science Computational Centre at the University of Queensland (Australia). The authors thank D. Breuer, T. Burghardt, N. Coltice, S. Ferrachat, R. Hendel, W. Jacoby, G. Jentzsch, and L. Viereck-Götte for helpful discussions. Comments from D. Murphy and an anonymous reviewer improved the manuscript and were highly appreciated.

References

Albarède F (2001) Radiogenic in growth in systems with multiple reservoirs: applications to the differentiation of the mantle-crust system. Earth and Planetary Science Letters 189: 59–73

Albarède F, van der Hilst RD (2002) Zoned mantle convection. Philosophical Transactions of the Royal Society of London: A 360: 2569–2592

Allègre CJ (2002) The evolution of mantle mixing. Philosophical Transactions: Mathematical, Physical and Engineering Sciences 360(1800): 2411–2431

Allègre CJ, Hamelin B, Provost A, Dupre B (1987) Topology in isotopic multispace and origin of mantle chemical heterogeneities. Earth and Planetary Science Letters 81(4): 319–337

Allègre CJ, Hofmann AW, O'Nions K (1996) The argon constraints on mantle structure. Geophysical Research Letters 23: 3555–3557

Allègre CJ, Turcotte DL (1986) Implications of a two-component marble-cake mantle. Nature 323: 123–127

Anderson OL (1998) The Grüneisen parameter for iron at outer core conditions and the resulting conductive heat and power in the core. Physics of the Earth and Planetary Interiors 109: 179–197

Andreasen R, Sharma M (2006) Solar nebula heterogeneity in p-process Samarium and Neodymium isotopes. Science 314(5800): 806–809

Arndt NT (2004) The Precambrian Earth: Tempos and events. In: Eriksson PG, Altermann W, Nelson DR, Mueller WU, Catuneanu O Developments in Precambrian Geology, 12, Elsevier, 155–158

Arrhenius G, Lepland A (2000) Accretion of Moon and Earth and the emergence of life. Chemical Geology 169: 69–82

Ballentine CJ, van Keken P, Porcelli D, Hauri EH (2002) Numerical models, geochemistry and the zero-paradox noble-gas mantle. Philosophical Transactions of the Royal Society of London: A 360: 2611–2631

Baumgardner JR (1983) A three-dimensional finite element model for mantle convection, Los Angeles: University of California

Baumgardner JR, Frederickson PO (1985) Icosahedral discretization of the 2-sphere. Siam Journal on Numerical Analysis 22(6): 1107–1115

Becker TW, Kellogg JB, O'Connell RJ (1999) Thermal constraints on the survival of primitive blobs in the lower mantle. Earth and Planetary Science Letters 171: 351–365

Bercovici D, Karato S-I (2003) Whole-mantle convection and the transition-zone water filter. Nature 425: 39–44

Boehler R (2000) High-pressure experiments and the phase diagram of lower mantle and core materials. Reviews of Geophysics 38(2): 221–245

Boyet M, Carlson RW (2005) ^{142}Nd evidence for early (>4.53 Ga) global differentiation of the silicate Earth. Science 309: 576–581

Breuer D, Spohn T (1995) Possible flush instability in mantle convection at the Archaean–Proterozoic transition. Nature 378: 608–610

Bunge H-P, Baumgardner JR (1995) Mantle convection modeling on parallel virtual machines. Computers in Physics 9(2): 207–215

Bunge H-P, Richards MA, Baumgardner JR (1997) A sensitivity study of three-dimensional spherical mantle convection at 10^8 Rayleigh number: effects of depth-dependent viscosity, heating mode, and an endothermic phase change. Journal of Geophysical Research 102(B6): 11991–12007

Campbell IH (1998) The Earth's Mantle: Composition, structure and evolution. In: Jackson I, Cambridge University Press, Cambridge, 259–310

Canup RM (2004) Simulations of a late lunar-forming impact. Icarus 168(2): 433–456

Carlson RW, Boyet M, Horan M (2007) Chondrite Barium, Neodymium, and Samarium isotopic heterogeneity and early Earth differentiation. Science 316(5828): 1175–1178

Coltice N, Ricard Y (2002) On the origin of noble gases in mantle plumes. Philosophical Transactions of the Royal Society of London: A 360: 2633–2648

Condie KC (1997) Plate Tectonics and Crustal Evolution. Butterworth-Heinemann

Davaille A (1999) Simultaneous generation of hotspots and superswells by convection in a heterogeneous planetary mantle. Nature 402: 756–760

Davies GF (2005) A case for mantle plumes. Chinese Science Bulletin 50(1): 1–14

DeVolder B, Glimm J, Grove J, Kang Y, Lee Y, Pao K, Sharp DH, Ye K (2002) Uncertainty quantification for multiscale simulations. Journal of Fluids and Engineering 124: 29–41

Dixon JE, Dixon TH, Bell DR, Malservisi R (2004) Lateral variation in upper mantle viscosity: role of water. Earth and Planetary Science Letters 222(2): 451–467

Dziewonski AM, Anderson DL (1981) Preliminary reference Earth model. Physics of the Earth and Planetary Interiors 25: 297–356

Elkins-Tanton LT, Parmentier EM, Hess PC (2003) Magma ocean fractional crystallization and cumulate overturn in terrestrial planets: Implications for Mars. Meteoritics and Planetary Science 38(12): 1711–1875

Ferrachat S, Ricard Y (2001) Mixing properties in the Earth's mantle: Effects of the viscosity stratification and of oceanic crust segregation. Geochemistry Geophysics Geosystems 2: 1013, doi: 10.1029/2000GC000092

Glatzmaier GA (1988) Numerical simulations of mantle convection: Time-dependent, three-dimensional, compressible, spherical shell. Geophysical and Astrophysical Fluid Dynamics 43: 223–264

Gonnermann HM, Mukhopadhyay S (2007) Non-equilibrium degassing and a primordial source for helium in ocean-island volcanism. Nature 449: 1037–1040

Gordon RG, Jurdy DM (1986) Cenozoic global plate motions. Journal of Geophysical Research 91: 12389–12406

Gottschaldt K-D (2003) Vermischung in 3D sphärischen Konvektionsmodellen des Erdmantels, Jena: Friedrich-Schiller-Universität

Gottschaldt K-D, Walzer U, Hendel RF, Stegman DR, Baumgardner JR, Mühlhaus H-B (2006) Stirring in 3-d spherical models of convection in the Earth's mantle. Philosophical Magazine 86(21–22): 3175–3204

Grand SP, van der Hilst RD, Widiyantoro S (1997) Global seismic tomography: a snapshot of convection in the Earth. GSA Today 7: 1–7

Hanan BB, Blichert-Toft J, Pyle DG, Christie DM (2004) Contrasting origins of the upper mantle revealed by hafnium and lead isotopes from the Southeast Indian Ridge. Nature 432: 91–94

Hart S (1984) A large-scale isotope anomaly in the southern hemisphere mantle. Nature 309: 753–757

Helffrich GR, Wood BJ (2001) The Earth's mantle. Nature 412: 501–507

Hirose K (2002) Phase transitions in pyrolitic mantle around 670 km depth: Implications for upwelling of plumes from the lower mantle. Journal of Geophysical Research 107(B4): 2078, doi:10.1029/2001JB000597

Hirose K (2006) Postperovskite phase transition and its geophysical implications. Reviews of Geophysics 44(2005RG000186): RG3001

Hirth G, Kohlstedt DL (1996) Water in the oceanic upper mantle: implications for rheology, melt extraction and the evolution of the lithosphere. Earth and Planetary Science Letters 144: 93–108

Hofmann AW (1988) Chemical differentiation of the earth – The relationship between mantle, continental crust, and oceanic crust. Earth and Planetary Science Letters 90(3): 297–314

Hofmann AW (1997) Mantle geochemistry: the message from oceanic volcanism. Nature 385: 219–229

Holland G, Ballentine CJ (2006) Seawater subduction controls the heavy noble gas composition of the mantle. Nature 441: 186–191

Karato S-I, Riedel MR, Yuen DA (2001) Rheological structure and deformation of subducted slabs in the mantle transition zone: implications for mantle circulation and deep earthquakes. Physics of the Earth and Planetary Interiors 127: 83–108

Kellogg JB, Jacobsen SB, O'Connell RJ (2002) Modeling the distribution of isotopic ratios in geochemical reservoirs. Earth and Planetary Science Letters 204: 183–202

Kellogg LH, Hager BH, van der Hilst RD (1999) Compositional stratification in the deep mantle. Science 283: 1881–1884

Kleine T, Mezger K, Palme H, Münker C (2004) The W isotope evolution of the bulk silicate Earth: constraints on the timing and mechanisms of core formation and accretion. Earth and Planetary Science Letters 228(1–2): 109–123

Labrosse S (2003) Thermal and magnetic evolution of the Earth's core. Physics of the Earth and Planetary Interiors 140(1): 127–143

Labrosse S, Hernlund JW, Coltice N (2007) A crystallizing dense magma ocean at the base of the Earth's mantle. Nature 450: 866–869

Manga M (1996) Mixing of heterogeneities in the mantle: Effect of viscosity differences. Geophysical Research Letters 23(4): 403–406

McNamara AK, Zhong SJ (2004) Thermochemical structures within a spherical mantle: Superplumes or piles? Journal of Geophysical Research 109: B07402

Meibom A, Anderson DL (2003) The statistical upper mantle assemblage. Earth and Planetary Science Letters 217: 123–139

Monnereau M, Yuen D (2007) Topology of the postperovskite phase transition and mantle dynamics. Proceedings of the National Academy of Sciences 104:9156–9161, doi:10.1073/pnas.0608480104

Monnereau M, Yuen D (2007) Topology of the postperovskite phase transition and mantle dynamics. PNAS

Montelli R, Nolet G, Dahlen FA, Masters G, Engdahl ER, Hung S-H (2004) Finite-frequency tomography reveals a variety of plumes in the mantle. Science 303: 338–343

Nakagawa T, Tackley PJ (2004) Effects of a perovskite-post perovskite phase change near core-mantle boundary in compressible mantle convection. Geophysical Research Letters 31(L16611)

Nolet G, Karato S-I, Montelli R (2006) Plume fluxes from seismic tomography. Earth and Planetary Science Letters 248: 685–699

O'Connell RJ, Gable CW, Hager BH (1991) Toroidal-poloidal partitioning of lithospheric plate motion. In: Sabadini K, Lambeck K, Boschi E Glacial Isostasy, Sea Level, and Mantle Rheology, Kluwer Academic Publishers, Dordrecht, 535–551

O'Neill HSC, Palme H, Jackson I (1998) The Earth's mantle: Composition, structure and evolution. Cambridge University Press, Cambridge, UK

Oldham D, Davies HW (2004) Numerical investigation of layered convection in a three-dimensional shell with application to planetary mantles. Geochemistry Geophysics Geosystems 5(12): Q12C04

Presnall DC, Gudfinnsson GH, Walter MJ (2002) Generation of mid-ocean ridge basalts at pressures from 1 to 7 GPa. Geochimica et Cosmochimica Acta 66(12): 2073–2090

Ramage A, Walthan AJ (1992) Iterative solution techniques for finite element discretizations of fluid flow problems. Copper Mountain Conference on Iterative Methods, Copper Mountain, Colorado

Ranen MC, Jacobsen SB (2006) Barium isotopes in chondritic meteorites: implications for planetary reservoir models. Science 314(5800): 809–812
Regenauer-Lieb K, Kohl T (2003) Water solubility and diffusivity in olivine: its role in planetary tectonics. Mineralogical Magazine 67(4): 697–715
Ritsema J, van Heijst HJ (2000) Seismic imaging of structural heterogeneity in Earth's mantle: evidence for large-scale mantle flow. Science Progress 83(3): 243–259
Ritsema J, van Heijst HJ, Woodhouse JH (1999) Complex shear wave velocity structure imaged beneath Africa and Iceland. Science 286(5546): 1925–1928
Rüpke L, Phipps-Morgan J, Hort M, Connolly J, Ranero C (2003) Serpentine and the chemical evolution of the earth's mantle. Geophysical Research Abstracts 5: 09637 See: http://www.cosis.net/abstracts/EAE03/09637/EAE03-J-09637.pdf
Schubert G, Turcotte DL, Olson P (2001) Mantle convection in the Earth and Planets. Cambridge University Press, Cambridge
Smolarkiewicz PK (1984) A fully multidimensional positive definite advection transport algorithm with small implicit diffusion. Journal of Computational Physics 54(2): 325–362
Solomatov VS (2000) Fluid dynamics of a terrestrial magma ocean. In: Canup RM, Righter K Origin of the Earth and Moon, University of Arizona Press, Tucson, 323–338
Stacey FD (1992) Physics of the Earth. Brookfield Press, Brisbane
Stegman DR, Richards MA, Baumgardner JR (2002) Effects of depth-dependent viscosity and plate motions on maintaining a relatively uniform mid-ocean ridge basalt reservoir in whole mantle flow. Journal of Geophysical Research 107(B6): 10.1029/2001JB000192
Su W-J, Woodward RL, Dziewonski AM (1994) Degree 12 model of shear velocity heterogeneity in the mantle. Journal of Geophysical Research 99(B4): 6945–6980
Tackley PJ (1996) Effects of strongly variable viscosity on three-dimensional compressible convection in planetary mantles. Journal of Geophysical Research 101(B2): 3311–3332
Tackley PJ (2000) Mantle convection and plate tectonics: Toward an integrated physical and chemical theory. Science 288: 2002–2007
Tackley PJ (2002) Strong heterogeneity caused by deep mantle layering. Geochemistry Geophysics Geosystems 3(4)
Tackley PJ, Nakagawa T, Hernlund JW (2007) Post-Perovskite: The last mantle phase transition. Geophysical Monograph Series 174: 229–247
Taylor SR, McLennan SM (1995) The geochemical evolution of the continental crust. Reviews of Geophysics 33(2): 241–265
Tolstikhin I, Hofmann AW (2005) Early crust on top of the Earth's core. Physics of the Earth and Planetary Interiors 148: 109–130
Trampert J, Deschamps F, Resovsky J, Yuen D (2004) Probabilistic tomography maps chemical heterogeneities throughout the lower mantle. Science 306: 853–856

Trendall AF (2002) Precambrian sedimentary environments: A modern approach to depositional systems. In: Altermann W, Corcoran PL IAS spec. publ., 44, Blackwell, 33–66

Turcotte DL, Schubert G (2002) Geodynamics. Cambridge University Press, Cambridge

van der Hilst RD (2004) Changing views on Earth's deep mantle. Science 306(5697): 817–818

van der Hilst RD, Widiyantoro S, Engdahl ER (1997) Evidence for deep mantle circulation from global tomography. Nature 386: 578–584

van Keken P, Ballentine CJ, Porcelli D (2001) A dynamical investigation of the heat and helium imbalance. Earth and Planetary Science Letters 171: 533–547

van Keken P, Zhong SJ (1999) Mixing in a 3D spherical model of present-day mantle convection. Earth and Planetary Science Letters 171: 533–547

van Keken PE, Ballentine CJ (1998) Whole-mantle versus layered mantle convection and the role of a high-viscosity lower mantle in terrestrial volatile evolution. Earth and Planetary Science Letters 156(1–2): 19–32

van Keken PE, King SD, Schmeling H, Christensen UR, Neumeister D, Doin MP (1997) A comparison of methods for the modeling of thermochemical convection. Journal of Geophysical Research 102(B10): 22477–22495

van Thienen P (2003) Evolving dynamical regimes during secular cooling of terrestrial planets: insights and inferences from numerical models, Universiteit Utrecht, Utrecht

Walzer U, Hendel R (2008) Mantle convection and evolution of growing continents. Journal of Geophysical Research 113: B09405, doi: 10.1029/2007JB005459

Walzer U, Hendel RF (1999) A new convection-fractionation model for the evolution of the principal geochemical reservoirs of the Earth's mantle. Physics of the Earth and Planetary Interiors 112: 211–256

Walzer U, Hendel RF, Baumgardner JR (2003) Viscosity stratification and a 3D compressible spherical shell model of mantle evolution. High Performance Computing in Science and Engineering 2003: 419–428

Walzer U, Hendel RF, Baumgardner JR (2004a) The effects of a variation of the radial viscosity profile on mantle evolution. Tectonophysics 384: 55–90

Walzer U, Hendel RF, Baumgardner JR (2004b) Toward a thermochemical model of the evolution of the Earth's mantle. High Performance Computing in Science and Engineering 2004: 395–454

Watson EB, Thomas JB, Cherniak DJ (2007) 40Ar retention in the terrestrial planets. Nature 449: 299–304

Weiss D, Bassias Y, Gautier I, Mennesier J-P (1989) Dupal anomaly in existence 115 ma ago: Evidence from isotopic study of the Kerguelen plateau (South Indian Ocean). Geochimica et Cosmochimica Acta 53: 2125–2131

Xie S, Tackley PJ (2004) Evolution of Helium and Argon Isotopes in a convecting mantle. Physics of the Earth and Planetary Interiors 146(3–4): 417–439

Yang W-S (1997) Variable viscosity thermal convection at infinite Prandtl number in a thick spherical shell, University of Illinois, Urbana-Champaign

Zaranek SE, Parmentier EM (2004) Convective cooling of an initially stably stratified fluid with temperature-dependent viscosity – Implications for the role of solid-state convection in planetary evolution. Journal of Geophysical Research 109(B3): B03409

Zerr A, Boehler R (1993) Melting of (Mg,Fe)SiO3-perovskite to 625 kilobars: Indication of a high melting temperature in the lower mantle. Science 262: 553–555

Zerr A, Boehler R (1994) Constraints on the melting temperature of the lower mantle from high-pressure experiments on MgO and magnesiowüstite. Nature 371: 506–508